DR CHIARA AMADORI (Orcid ID : 0000-0002-7220-442X)

Article type : Original Article

Restored topography of the Po Plain-Northern Adriatic region during the Messinian base-level drop - implications for the physiography and compartmentalisation of the paleo-Mediterranean basin

Chiara Amadori[1], Daniel Garcia-Castellanos[2], Giovanni Toscani[1], Pietro Sternai[3], Roberto Fantoni[4], Manlio Ghielmi[4] and Andrea Di Giulio[1]

[1]Department of Earth and Environmental Sciences, University of Pavia, 27100 Pavia, Italy. (corresponding author) chiara.amadori01@universitadipavia.it; giovanni.toscani@unipv.it; andrea.digiulio@unipv.it

[2]Instituto de Ciencias de la Tierra Jaume Almera, ICTJA-CSIC, 08028 Barcelona, Spain. danielgc@ictja.csic.es

[3]Department of Earth Sciences, University of Geneva, 1205 Geneva, Switzerland. pietro.sternai@unige.ch

[4]Eni Upstream & Technical Services, 20097 San Donato Milanese, Italy. roberto.fantoni@eni.com; manlio.ghielmi@eni.com

ABSTRACT

The Messinian Salinity Crisis (MSC) involved the progressive isolation of the Mediterranean Sea from the Atlantic between 5.97-5.33 Ma and a sea-level fall whose timing, modalities and magnitude remain actively debated. At that time, the central Mediterranean was undergoing strong tectonic activity due to the rollback of the Adria slab and eastward migration of the Apenninic belt. The combined effects of the post-evaporitic MSC sea-level drop and morpho-structural changes (due to the Intra-Messinian phase) resulted in a regional

This article has been accepted for publication and undergone full peer review but has not been through the copyediting, typesetting, pagination and proofreading process, which may lead to differences between this version and the Version of Record. Please cite this article as doi: 10.1111/bre.12302

unconformity, which shows erosive markers and conformable relationships with the Messinian and Mio-Pliocene boundary in the Po Plain and Northern Adriatic Foreland. Here, we produce a paleo-topographic reconstruction of the Po Plain-Northern Adriatic region (PPNA) during the Messinian peak desiccation event based on such regional unconformity. We mapped this surface through wells and 2D seismic data form Eni's private dataset. The unconformity shows V-shaped incisions matching present-day southern Alpine valleys and filled with Messinian post-evaporitic and Pliocene deposits, suggesting that the modern drainage network is at least of late Messinian age. The Messinian unconformity has been restored to its original state through flexural-backstripping numerical modelling. The resulting landscape suggests a maximum sea-level drop of 800-900 m during the MSC peak and is consistent with stratigraphic and sedimentologic data provided by previous works. The modelled shoreline separates the subaerially eroded land from an elongated basin composed by two *ca.* 400 and 1000 m deep depocenters during the maximum sea-level drop. These results suggest that the Mediterranean was split in at least three sub-basins subject to independent base-levels, fresh water budgets and flexural responses during the maximum lowstand.

INTRODUCTION

The Messinian Salinity Crisis (MSC) is one of the most extreme and debated Cenozoic environmental changes (Rouchy & Caruso, 2006; Roveri *et al.*, 2014a, b; Vai, 2016 and reference therein). Diagnostic evaporitic deposits (Selli, 1960; Hsü *et al.,* 1973, 1977; Müller & Mueller, 1991; Allen *et al.*, 2016) and erosional unconformities across the entire Mediterranean (Lofi *et al.*, 2005; Bertoni & Cartwright 2006; Lofi *et al.*, 2011a, b) enable to date this event between 5.33-5.97 Ma (Krijgsman *et al.*, 1999; Manzi *et al.*, 2013). Many of the erosional unconformities merge into a single polygenic surface (usually referred to as the Margin Erosional Surface – MES, Lofi *et al.*, 2005; CIESM, 2008, Lymer *et al.*, 2018) in the upstream of deep marginal and intermediate basins (Roveri *et al.*, 2014b; Lymer *et al.,* 2018), thereby providing evidence for erosion in the Mediterranean margin. Many of the key depositional units and erosional markers of the MSC, however, are buried underneath km-thick sedimentary units and currently located offshore (Lofi *et al*., 2011a, b; Urgeles *et al*., 2011; Gorini *et al*., 2015; Thinon *et al*., 2016), while accessible outcrops are strongly deformed by late-Cenozoic tectonics (e.g. Sicily, Butler *et al*., 1995; Caruso *et al*., 2015). Therefore, assessing the magnitude of the drawdown and the resulting paleogeography of the Mediterranean area during the MSC acme is still difficult (e.g. Hsü *et al*., 1977; Cita & Corselli, 1990; Blanc, 2006; Meijer & Krijgsman 2005; Jolivet *et al*., 2006; Bache *et al*., 2012; Roveri *et al*., 2014a, b; Vai, 2016; Sternai *et al*., 2017). Previous numerical modelling produced quantitative estimates regarding sea-level and salinity variations, as well as the flexural response at the Mediterranean scale (Meijer *et al*., 2004; Meijer & Krijgsman 2005; Gargani & Rigollet, 2007; Govers, 2009). Given the regional length scales, these studies used relatively low-resolution Messinian key-horizons with minor geological control on the palinspastic retrodeformation or lithofacies record. Although the separation between the western and eastern Mediterranean basins by the Sicily sill is accepted (Gargani & Rigollet, 2007; Ryan, 2009; Micallef *et al.*, 2018), uncertainties exist regarding the central Mediterranean and, particularly, its northernmost sector, the Po Plain and Adriatic basin. During the Messinian, this sector of the Mediterranean was a complex puzzle of fragmented carbonate platforms, basins and outcropping Apennines which is challenging to restore at a regional scale (Jolivet *et al*., 2006; Patacca & Scandone 2007; Mantovani *et al.,* 2014; Matano *et al.,* 2014). Within this scenario, the possibility that smaller basins and their connections during the MSC has not been taken into account by previous numerical modelling studies.

We model the sea-level drop of the Po Plain-Northern Adriatic foreland basin (PPNA) during the Messinian based on its detailed stratigraphic record in order to better understand its connectivity with the rest of the Mediterranean Sea during the MSC. To this aim, we analyse public and private (courtesy of Eni Upstream) subsurface data and carry out a 3D reconstruction of the subaerial and submarine landscape of the Po Pain and Adriatic foreland during the MSC desiccation peak, i.e., after the MSC stage 1 according to the chronostratigraphy by Roveri *et al*. (2014a, b, 2016). We take advantage from high-resolution stratigraphic data (e.g. sedimentological, paleontological and geochemical data) and detailed geological constraints (e.g. seismic-based and well logs) for the study region also provided by recent works (Ghielmi *et al*., 2010, 2013; Rossi *et al*., 2015; Rossi, 2017; Rossi et *al*., 2018). We are able to (1) provide the paleotopography of the PPNA, which improves our understanding of the basin evolution and its relationships with the broader Mediterranean paleogeography during the MSC, and (2) recognize V-shaped valleys filled with Messinian post-evaporitic and Pliocene deposits in the seismic data along the southern Alps, which imply a syn-MSC or older age of the present-day southern Alpine river drainage pattern.

GEOLOGICAL SETTING

Tectonic shortening affected the PPNA at different times and with variable directions during the Cenozoic (e.g. Toscani *et al*., 2016). Since the middle-late Miocene, the thrust front of the Northern Apennine thrust-fold-belt bounds to the southwest the Po Plain and Northern Adriatic Foredeep Basins (Fantoni & Franciosi, 2010; Ghielmi *et al*., 2013; Rossi *et al*., 2015). The Western and Southern Alps bound the Western Po Plain foredeep basins to the north, while the PPNA is connected to the northeast to the Venetian-Friulian Basin (Fig. 1a).

During the Messinian, the whole Apennine thrust belt experienced a period of strong tectonic accretion, defined as Intra-Messinian phase (Ghielmi *et al*., 2010, 2013; Mantovani *et al.,* 2014; Matano *et al*., 2014). The PPNA was marked by a strong sedimentary and tectonic reorganization related to combined effects of the MSC drawdown and morpho-structual reshaping, resulting in an angular unconformity overlaid by post-evaporitic Messinian prograding systems or transgressive Pliocene deposits (Ghielmi *et al*., 2010, 2013; Rossi *et al*., 2015, 2018; Rossi, 2017). In seismic profiles on the basin margins, this unconformity shows erosive markers (truncation of the MSC lower evaporates or pre-MSC succession) at the base of forced regressive deltaic systems and predominantly conformable relationships basinward through the entire Messinian sequence and Mio-Pliocene boundary (Fig. 1c). Unlike the Western and Eastern Mediterranean offshore (Lofi *et al*., 2011a, b), the PPNA region was not a fully evaporative basin during the MSC (Ghielmi *et al.*, 2010, 2013), as suggested by the absence of halite and potassium-rich salts deposition in the entire Adriatic foreland (Ryan, 2009). Geophysical investigations in the Po Plain led Ghielmi *et al*. (2010, 2013) and Rossi *et al*. (2015) to reconstruct syn- and post-evaporitic lithofacies associations distribution maps (i.e. continental *vs* marine shelf-to-basin sediments), showing evidence for a thick coastal wedge where the complete Messinian succession is preserved, included pre-evaporitic deposits. Instead, in the northern and eastern Adriatic foreland, Messinian sediments are poorly preserved or lacking (Fig. 2a). In detail, cyclic gypsum and anhydrite deposits (maximum thickness in well ~250 m) are observed only in marine foreland shelves (along the northern margin of the PPNA) and hypersaline piggy-back basins on the Northern Apennine belt, overlain by post-evaporitic Messinian brackish sequences (Artoni *et al*., 2007, 2010; Ghielmi *et al*., 2010, 2013; Rossi *et al*., 2015; Pellen *et al*., 2017). In the deep part of the basin, the sedimentary sequence is only composed of siliciclastic deposits, also during the MSC post-evaporitic maximum desiccation phase (Ghielmi *et al.*, 2010). According to this geological setting, the Po Plan-Adriatic basin can be defined as intermediate basin *sensu* Lymer *et al*. (2018). Lymer *at al*. describe intermediate basins as located between peripheral shallow basins (with presence of lower evaporates only overlain by Pliocene deposits) and deep basins (with presence of thick halite), covering a wide range of both bathymetries and MSC deposits.

Late Messinian incised valleys in the Venetian-Friulian Basin onshore and offshore (Donda *et al*., 2013; Toscani *et al*., 2016; Zecchin *et al*., 2017) led to suggest a maximum relative sea-level drop in the Northern Adriatic region of more than 100-200 m during MSC acme, but not exceeding 900 m (Ghielmi *et al.,* 2013). This is in divergence with previous interpretations from Roveri *et al.* (2014a, b, 2016) based on modeling submarine dense water cascading from the shelf areas producing canyons without the need of significant drawdown. Roveri *et al*. extended the proposal of a relatively minor MSC sea-level drop (100-200 m) to the entire Mediterranean, in contrast with other estimates suggesting between 1300 and 2000 m of sea-level drop (Ryan, 1976; Stampfli & Hocker, 1989; Clauzon *et al*., 1996; Krijgsman *et al*., 1999; Blanc, 2000; Meijer & Krijgsman, 2005; Maillard & Mauffret, 2006; Urgeles *et al*., 2011; Cameselle & Urgeles, 2016; see Vai, 2016 for a review; Sternai *et al.*, 2017).

DATASETS AND METHODS

We use public (ViDEPI Project, http://www.videpi.com) and private (courtesy of Eni Upstream) 2D seismic reflection profiles and hydrocarbon wells data from the PPNA region (Fig. 3) to reconstruct the 3D surface of the unconformity formed during the MSC acme. The seismic dataset is composed of about 8000 km of seismic reflection profiles (both onshore and offshore) and it has been integrated with published data both for the western (Bigi *et al*., 1992; Fantoni *et al*., 2001, 2004; Mosca, 2006; Rossi, 2017) (Fig. 3b, d) and eastern (Toscani *et al*., 2016) parts of the study area (Fig. 3c). Wells data (Eni private database and ViDEPI project) include both stratigraphy and well logs from about 200 wells (Fig. 3a).

The Messinian key-horizon has been interpreted in 2D seismic lines and recognised in well logs. In order to create a 3D time-surface from scattered data, we used the Delaunay triangulation method and smoothed the resulting surface using a characteristic length scale of 3 km to remove asperities due to the noise in the data and interpolation method. The resultant 3D time-surface has been depth-converted using a homogeneous seismic wave velocity value of 2000 m/s, an average value obtained considering both confidential (time-velocity tables of ENI wells) and public data (e.g. Bresciani & Perotti, 2014; ISPRA, 2015; Molinari *et al*., 2015).

In addition to the MES, this research involves two other surfaces: (i) the Mesozoic Carbonates top surface in depth domain, taken as the fully compacted “basement” for the backstripping analysis (digitalized after Turrini *et al*., 2014, 2016; Toscani *et al*., 2016) (Fig. 1b, c) and (ii) the present-day topography (after GTOPO30; https://lta.cr.usgs.gov/GTOPO30) corrected to account for Pleistocene erosion of the European Alps and the related unload and isostatic adjustment (after Sternai *et al*., 2012). The top of the pre-collisional carbonate basement is an important surface for hydrocarbon because it corresponds to the top of a deep oil play and the major seismic marker for the related structure interpretation (Turrini *et al.,* 2014, 2016).

The restoration of the regional paleo-topography during the maximum MSC drawdown was obtained following the workflow outlined in figure 4a and using the TISC software (Garcia-Castellanos, 2002; Garcia-Castellanos *et al*., 2003). We account for sediment decompaction and for the 2D (planform) flexural isostatic adjustment associated with unloading by the removal of post-Messinian sediments and the missing water column during the MSC acme (Fig. 4). In summary the workflow involves: (i) removal of the shallowest stratigraphic unit and calculation of the flexural-isostatic response, (ii) decompaction of the underlying sedimentary units, (iii) removal of the water layer and calculation of the corresponding flexural-isostatic response. This is a standard methodology in subsidence basin analysis (Allen & Allen, 1990; Bell *et al*., 2014). Decompaction is conducted by calculating near-surface porosity, decay constants and bulk densities for lithologies observed in wells and also using the relationships provided by Sclater & Christie (1980) (see Tab.1). We assigned uniform surface porosity, bulk density and porosity-depth exponential coefficient to the analysed volumes. We disregard gradual sediment compaction because the model is time-independent and we are not interested on the evolution of subsidence but on the total amount of post-Messinian subsidence. We also disregard non-uniform grain size or sediment facies distribution because of lack of deep wells with pre-MSC detailed data covering the entire region. Following previous numerical models on MSC river erosion and water/evaporation budget, we assume that the sea-level before the MSC was close to the present-day one (Loget et *al.,* 2005; Blanc, 2006; Gargani & Ricollet, 2007; Miller *et al*., 2005). The most representative lithologies within the Paleogene-late Messinian sediments (volume to be decompacted) are marine marls (i.e., Scaglia Formation and Gallare Group) and sandstones (i.e., Gonfolite Group and latest Tortonian-syn-evaporitic Messinian turbidites of Bagnolo Formation) with an averaged lithology-type of 75% shale and 25% sand (Tab. 1). The upper volume to be removed is mostly represented by km-thick Plio-Pleistocene turbidites (variable in clay content) and fine-grained foreland deposits (i.e. Zanclean marine shales). The averaged lithology-type is similar to the "Shaley Sandstone" defined by Sclater & Christie (1980 (Tab. 1). The density of both the removed seawater and the remaining water volume during the MSC drop is assumed to be 1030 kg/m^3 like the current average seawater density at the surface (Beicher, 2000). Finally, the basement density was set to 2850 kg/m^3 (Ebbing *et al.,* 2001).

The restoration of the tectonic deformation of the basin was carried out removing the vertical component of the main Pliocene-Pleistocene thrusts and anticlines of the Northern Apennines and Western and Southern Alps, according to published uplift data (Scrocca *et al*., 2007; Toscani *et al*., 2014; Maesano *et al*., 2015; Bresciani & Perotti, 2014; Tab. 2) (Fig. 5a). In performing this operation, we neglect horizontal deformation given that previous works suggest between 10 and 20 km of average horizontal shortening (~10% with respect to the basin width) along the Northern Apennine front in the Po basin since the late Messinian (Fig. 5b) (Perotti, 1991; Bigi *et al*., 1995; De Donatis, 2001; Toscani *et al*., 2014), which translates into minor strain at the basin scale. This is also in agreement with the regional-scale Apennine eastward migration (since ~5 Ma up to present position) reconstructed by Carminati *et al*. (2010). We assume such limited shortening does not affect the modeling.

RESULTS

The depth-converted late Messinian unconformity of the PPNA with 500 m contouring is shown in Fig. 6. The overall northern margin of the PPNA appears incised by *ca.* N-S and NW-SE trending valleys. In detail, in the Southern Alpine sector the incisions show steep V-shape morphologies (Figs. 6, 7), cutting upslope Oligocene-Late Miocene sediments (Fig. 7c). These canyons are filled with Messinian post-evaporitic fluvial conglomerates of the Sergnano Fm and Plio-Pleistocene turbidites (Fig. 7c). The volume to be removed is mainly composed by km-thick Plio-Pleistocene turbidites, dominant with respect to the late Messinian deposits. From the

Alpine land outcrops to the deep Po Plain, the Messinian succession appears incomplete, which is likely due to erosion and forced regression of the fluvio-deltaic systems during base-level lowering, as also pointed out by Rossi *et al.* (2015, 2018). In the eastern Adriatic foreland ramp, late Messinian sediments are poorly preserved or completely lacking (Fig. 2a). From 3D depth-reconstruction, these fluvial incisions have propagated at least 50 km inland, with the maximum depth reaching ~1 km in the central Po Plain (Figs. 6, 7a, b).

Parametric Study for the backstripping analysis

In order to test the sensibility to the input parameters (Tab. 3) and investigate different scenarios, we run a series of flexural-backstripping calculations looking for the best fit model with respect to the constrains provided by the data described in section Datasets and methods. In particular, in this section, we explore the sensitivity of model predictions in terms of the restored palaeo-shoreline position and the fit to the geological constraints to input parameters such as:

i) the amount of sea-level lowering, i.e., -200/-850/-1500 m to account for previously proposed MSC scenarios (e.g.; Ryan & Cita, 1978; Gargani, 2004; Manzi, 2005; Urgeles *et al*., 2011; Ghielmi *et al*., 2013; Roveri *et al*., 2014a, b),

ii) the lithospheric elastic thickness, *Te*, i.e., 10, 20, 45 km to account for plausible rheological conditions of the Adriatic continental basement (Moretti & Royden, 1988; Royden, 1988; Kruse & Royden, 1994; Kroon, 2002; Barbieri *et al*., 2004) and

iii) different lithologic characteristics of the sediments, in order to test how different sand-clay proportions affect the basement isostatic response.

The effect on the lithospheric post-Messinian vertical motions by the sea-level drop and elastic thickness variations appear as the most relevant (Fig. 8), while, varying only the porosity of the pre- and post- Messinian sediment volumes imply variations in the estimates by less than 100 m (Tab. 3). The estimated coastline location also depends primarily on the morphology of the basin and its slope. In the Adriatic foreland, the horizontal position of the shoreline shifts by up to ~150 km for sea-level drop >1km (Fig. 8c) due to the low basin slope. The steeper northern basin margin implies limited migration of the shoreline if the sea-level drop is ≤800-900 m, while a significant basinward migration of the coastline is observed for imposed drawdown > ~1.5 km (Fig. 8c, d, e). We remark that, overall, sea-level changes smaller than 50 m do not significantly affect the results of the backstripping analysis. For this reason, model predictions for each sea-level drop can be extended within a ±50 m interval.

Preferred Model

Our preferred reconstruction of the late Messinian unconformity within the PPNA basin accounts for an 850 m sea-level drop, *Te* equal to 20 km, decompacted sediments made of 75% clay and 25% sand and bulk density of volume to be removed of 2115 kg/m^3 (Tab. 1 and Fig. 9). These input parameter values are supported by previous studies or direct analysis on the region. For instance, the selected northern Adria plate lithospheric elastic thickness is consistent with results from Moretti & Royden (1988), Royden (1988) and Barbieri *et al*. (2004) and the lithology parameters are averaged from the deepest drilling and log analyses. The imposed amount of drawdown improves the fit between the modelled shoreline and sedimentologic constrains, i.e., coastal wedge position, fluvial drainage network, erosional surface (Fantoni *et al.,* 2001, Ghielmi *et al.*, 2010, 2013; Rossi *et al.*, 2015; Rossi, 2017; Rossi *et al.*, 2018) (Figs. 2, 9b, c) and continental *vs* marine shelf-to-basin facies boundary from the facies associations distribution map of the post-evaporitic sequence published by Ghielmi *et al.* (2010, 2013) (Fig. 9a). In addition, the output is consistent with the maximum base-level lowering of 900 m, as estimated by Ghielmi *et al.* (2013) through local investigations within the Po-Plain onshore (but never extended throughout the Po Plain western sector and Northern Adriatic offshore).

According to our preferred model, the PPNA region was a narrow basin with two definite submarine depocenters during the maximum Messinian drawdown. In the western Po Plain, the depocenter was nearly 400 m deep, while a wider WNW-ESE trending and ~1000 m deep depocenter was located to the east, where the maximum isostatic uplift occurred (~995 m, Fig. 10). Terrigenous turbidite deposition was enhanced in both sub-basins during Messinian time by the exposure of the pre-Messinian shelf (Fig. 9c) and by the accelerated erosion of the surrounding belts. To the NE, the Venetian-Friulian Basin is subaerially exposed during the maximum Messinian sea-level drop, a result that agrees with the proposed fluvial origin of the incised valleys and dendritic drainage network in the present-day onshore and offshore subsurface (Donda *et al.*, 2013; Ghielmi *et al*. 2010, 2013; Toscani *et al.*, 2016; Zecchin *et al.*, 2017) (Fig. 9b). Further to the east, a vast portion of the Mesozoic Istrian-Dalmatian platform, located in present-day Croatia region (Fig. 1a) and the Adriatic Sea, were subaerially exposed, which is also in agreement with previous works (Velić *et al.*, 2015) (Figs. 2a, 9a).

DISCUSSION

The timing of the end of the Southern Alpine tectonic deformation is well defined by seismic reflection profiles and exploration wells showing that Messinian post-evaporitic deposits (i.e., fluvio-deltaic forced regressive systems, Sergnano Fm.) and early Pliocene turbidite units are mostly undeformed (Pieri & Groppi, 1981; Fantoni *et al.*, 2001, 2004; Livio *et al.*, 2009; Rossi, 2017) (Fig. 7c). Additionally, the good fit between the subsurface incised valleys and the present-day river network flowing into the Po River alluvial plain reveals that the southern Alpine drainage pattern ~6 million years ago was very similar to the modern configuration (Fig. 7). Moreover, the equivalent spatial fit in the alluvial plain might possibly be due to the differential subsidence between the siliciclastic- and mud-filled incised valleys and their interfluves (Fig. 7c). One may interpret that the erosional features recognized below the central Southern Alps (Figs. 6, 7) testify that the margin underwent subaereal erosion as the base level dropped by hundreds of meters during the MSC. The Alpine rivers carved V-shaped valleys up to 1 km deep across the modern Po Basin and incised at least 50 km far into the Alps. Regressive erosion due to the Messinian drawdown shaped the cryptodepressions (*sensu* Bini *et al*., 1978) that today confine the glacial Alpine lakes of Northern Italy (e.g. Maggiore, Lugano, Como, Iseo and Garda lake) as first suggested by Bini *et al*. (1978), Finckh, (1978), Rizzini & Dondi, (1978). Similarly, several canyons that underlie current valleys have been documented all around the Mediterranean marginal regions, such as in the Nile, Rhone, Var Valleys, Alboran sill and the Ebro River (Chumakov, 1973; Barber, 1981; Clauzon, 1982; Loget *et al*., 2005, 2006; Urgeles *et al.,* 2011).

The main features of the restored late Messinian landscape of the PPNA region are two major depocenters subject to turbiditic deposition throughout the Messinian, rimmed by exposed marine shelves and localized hypersaline basins, in agreement with previous studies by Artoni *et al*. (2007, 2010) and Rossi *et al*. (2015) (Fig. 2, Fig. 9). The proposed ~850 m drop is significantly lower than the 1300-2000 m drawdown suggested by several authors. Among them Ryan (1976), Blanc (2000), Gargani (2004), Meijer & Krijgsman (2005), Gargani & Rigollet (2007), Sternai *et al*. (2017) sustain a kilometer sea-level drop on the basis of numerical modelling. Although Ryan & Cita (1978), Stampfli & Hocker (1989), Clauzon *et al*. (1996), Maillard & Mauffret (2006), Bache *et al*. (2009), Urgeles *et al*. (2011), Cameselle & Urgeles (2016) have revealed depositional processes associated with emersion of continental margins (e.g. Gulf of Lions, Valencia-Ebro margin) compatible with ~1500 m base-level fall, also by morphological evidences from seismics and well data.

Thus, we support the PPNA region as a restricted elongated foreland basin physically disconnected from the rest of the Mediterranean during the MSC post-evaporitic acme and subject to an independent hydrological balance in a way similar to that discussed by Blanc (2006) and Bache *et al*. (2012). This imposed a geomorphological base level in our study region shallower than that in the west and east Mediterranean sub-basins. Regarding the location of the morphological high separating the PPNA basin from the rest of the Mediterranean, the Adria foreland offshore offers a complex distribution of carbonate platforms and tectonic deformations suitable to sustain the hypothesis of at least one major paleo-sill in the area. For instance, in the central Adriatic Sea there is an important alignment of structural highs deformed during the Oligo-Miocene accompanied by halokinetic activity (Pikelj *et al.,* 2015) (also known as the Mid-Adriatic Ridge), although growth strata above Messinian evaporates show higher uplift activity during Plio-Pleistocene time (Scisciani & Calamita, 2009; Del Ben *et al.*, 2010). The region of the Apulian platform in the southern Adriatic Sea, however, is probably the best candidate for the location of the barrier separating the Apennine foredeep during the MSC desiccation peak from the rest of the Mediterranean. Cita & Corselli (1990), Clauzon *et al.* (2005), Bache *et al.* (2012), Santantonio *et al.* (2013), and Pellen *et al.* (2017) inferred that a divide was probably located between the present-day Gargano-Pelagosa region in the southern Adriatic Sea. Seismic data and well log analysis of southern Italy onshore and offshore (de Alteriis, 1995; Scrocca, 2010; Santantonio *et al.*, 2013; Pellen *et al.*, 2017) reveal a submarine high carbonate structure (cropping out in the Puglia region) with a stratigraphic hiatus and an erosive surface on Messinian evaporites, that further supports the paleogeographic reconstruction published by Vai (2016).

Although the timing of closure and re-opening of the southern Adriatic sill during the late Messinian is beyond the purpose of this work, the presence of marine bio-events (e.g. the first occurrence of *Turborotalita multiloba* and the *Neogloboquadrina acostanesis* sx/dx coiling change) in the pre-MSC sequences (Sierro *et al.*, 2001; Blanc-Valleron *et al.*, 2002; Gennari *et al.*, 2013; Caruso *et al.*, 2015), the reconstruction of the near Tertiary Piedmont Basin (TPB) (Fig. 1a) based on the Lower Evaporites gypsum (Dela Pierre, 2011) and the quasi-uniform $^{87}Sr/^{86}Sr$ values of the Lower Evaporites throughout the Mediterranean (Roveri *et al.*, 2014b; Schildgen *et al.*, 2014) suggest that the Po-Adriatic basin was connected to the rest of the Mediterranean at least during the pre-evaporitic and syn-evaporitic phases. The isolation of the PPNA basin from the Mediterranean occurred only after the deposition of the Lower Evaporites, that is during the maximum sea-level drop correlated with the TG12 or both TG12 and TG14 glacial intervals (Krijgsman & Meijer, 2008; Cosentino *et al.*, 2013) is still consistent with our preferred model.

This, however, implies an abrupt change in the integrated balance between river discharge, precipitation, evaporation and uplift rate to explain the rapid base level change. A positive freshwater budget may prevent salt saturation, explaining why halite or other high soluble K-rich salts did not accumulate in the entire Adriatic region during MSC. The PPNA syn- and post-evaporitic Messinian deposits may indeed reflect a complex equilibrium between high fresh-water input provided by the large rivers draining the Alpine belt and the progressive increase in salinity due to the MSC. This would cause precipitation of gypsum and anhydrite only in restricted basins in the Northern Apennine, like the Tertiary Piedmont basin, piggy-back basin, and very localized sectors of the Po Plain-Northern Adriatic shelf (Rossi *et al*., 2002; Artoni *et al*., 2007, 2010; Dela Pierre, 2011; Ghielmi *et al*., 2013; Rossi *et al*., 2015), coeval with siliciclastic deposition in the residual, deep depocenters (Ghielmi *et al*., 2010, 2013; Rossi *et al*., 2015).

CONCLUSIONS

The restored landscape of the PPNA region during the maximum MSC sea-level drop (Fig. 9) allows outlining the following conclusions.

- The flexural-backstripping modelling best matches the available subsurface stratigraphic and facies distribution data when an 800-900 m drawdown is imposed; thus, the sea-level fall related to the MSC maximum lowstand in the study area is smaller than what was inferred for the eastern and western Mediterranean (1300 m or more), but also significantly larger than what was proposed by Roveri *et al*. (2014a, b, 2016) for the entire Mediterranean area (about 200 m).
- This result implies that, at a broader scale, during maximum sea-level fall, the Mediterranean was divided into at least three sub-basins (the two major Western and Eastern Mediterranean Basins and PPNA) with independent base-level evolutions and water budgets. The separation from the rest of the Mediterranean can partly explain the lack of halite and potassium-rich salts in the Po Plain area and Adriatic Sea.

- The present-day fluvial network flows directly above buried incised valleys into the Southern Alpine basement below the Po Plain. The match in the flat plain is probably due to differential compaction of sediments between incised valley fills and interfluves. This suggests that the present fluvial network draining the Southern Alps can be dated back to at least the late Messinian.

Finally, based on our results, we suggest that caution should be used in performing analyses addressing the amount of drawdown during the MSC at the whole Mediterranean scale and support, for this purpose, the generation and use of high-resolution stratigraphic data (e.g. sedimentological, paleontological and geochemical data) and/or models (i.e. seismic-based constrained by well log data).

ACKNOWLEDGEMENTS

Eni Upstream is acknowledged for the permission to consult its reflection seismic profiles dataset. This paper is the result of the Amadori PHD research project funded by the University of Pavia, the COST Action Network MEDSALT (CA15103) and by the Spanish Government project MITE (CGL2014-59516). The authors wish to thank Angelo Camerlenghi, Massimo Zecchin and Christian Gorini for their constructive comments to the early version of the manuscript. Above all, we wish to thank Clara R. Rodriguez, Gael Lymer and one anonymous reviewer for their very helpful comments and refinements to the manuscript. Halliburton and Platte River Associates Inc. are kindly acknowledged for providing software licenses. Midland Valley Exploration Ltd. is kindly acknowledged for MOVE software licenses provided to the University of Pavia within the ASI (Academic Software Initiative). Special thanks are extended to the entire MEDSALT group for the useful discussions and support. Pietro Sternai is grateful to the Swiss NSF (Ambizione grant PZ00P2_168113/1).

REFERENCES CITED

ALLEN, P.A. & ALLEN, J.R. (1990) Basin Analisis: Principles & Applications. *Blackwell Scientific Publications*. Oxford. 451 pp.

ALLEN, H., JACKSON C. A-L. & FRASER A.J. (2016) Gravity-driven deformation of a youthful saline giant: the interplay between gliding and spreading in the Messinian basin of the Eastern Mediterranean. Petroleum Geoscience, 22, 4:340. doi:10.1144/petgeo2016-034

ARTONI, A., RIZZINI, F., ROVERI, M., GENNARI, R., MANZI, V., PAPANI, G., BERNINI, M. & ROSSI, M. (2007) Tectonic and Climatic Controls on Sedimentation in late Miocene Cortemaggiore Wedge-Top Basin (Northwestern Apennines, Italy). In: *Thrust Belts and Foreland Basins. From Fold Kinematics to Hydrocarbon Systems* (Ed. By Lacombe O., Lavé J., Roure F. & Vergés J), *Frontiers in Earth Sciences Series, Springer, Heidelberg*. 431-456.

ARTONI, A., BERNINI, M., PAPANI, G., RIZZINI, F., BARBACINI, G., ROSSI, M., ROGLEDI, S. & GHIELMI, M. (2010) Mass-transport deposits in confined wedge-top basins: surficial processes shaping the Messinian orogenic wedge of Northern Apennine of Italy. *Italian Journal of Geosciences*, 129 (1), 101-118.

BACHE, F., OLIVET, J. L., GORINI, C., RABINEAU, M., BAZTAN, J., ASLANIAN, D. & SUC, JP. (2009) Messinian erosional and salinity crises: View from the Provence Basin (Gulf of Lions, Western Mediterranean). *Earth and Planetary Science Letters*, 286, 139-157.

BACHE, F., POPESCU, S-M., GORINI, C., SUC, J-P., CLAUZON, G., OLIVET, J-L., RUBINO, J-L., MELINTE-DOBRINESCU, M.M., JOLIVET, L., JOUANNIC, G., LEROUZ, E., ASLANIAN, D., DOS REIS, A.T., MOCOCHAIN, L., DUMURDZANOV, N., ZAGORCHEV, I., SOKOUTIS, V.S., CSATO, I., UCARKUS, G. & CAKIR, Z. (2012) A two steps process for the reflooding of the Mediterranean after the Messinian Salinity Crisis. *Basin Research*, 24, 125-153.

BARBER, P.M. (1981) Messinian subaerial erosion of the Proto-Nile delta. *Marine Geology*, 44, 253–272.

BARBIERI, C., BERTOTTI, G., DI GIULIO, A., FANTONI, R. & ZOETEMEIJER, R. (2004) Flexural response of the Venetian) foreland to the Southalpine tectonics along the TRANSALP profile. *Terra Nova*, 16, 273-280.

BEICHER, R. J. (2000) Physics for Scientists and Engineers. Orlando: Saunders College. 5th edition, p. 1288.

BELL, R.E., JACKSON, C.A-L., ELLIOT, G.M., GAWTHORPE, R.L., SHARP, I.R. & MICHELSEN, L. (2014) Insights into the development of major rift-related unconformities from geologically constrained subsidence modelling: Halten Terrace, offshore mid Norway. *Basin Research*, 26, 203-224.

BERTONI, C. AND CARTWRIGHT, J.A (2006) Controls on basinwide architecture of late Miocene (Messinian) evaporites on the Levant margin (Eastern Mediterranean). *Sedimentary Geology*, 188-189, 93-114.

BIGI, G., COSENTINO, D., PAROTTO, M., SARTORI, R. & SCANDONE, P. (1992) Structural Model Of Italy. Scale 1:500,000. *Quaderni Ricerca Scientifica*, 3, 114.

BIGI, S., CALAMITA, F., CELLO, G., CENTAMORE, E., DEIANA, G., PALTRINIERI, W. & RIDOLFI, M. (1995) Evoluzione messiniano-pliocenica del sistema catena-avanfossa nell'area marchigiano-abruzzese esterna. *Studi Geologici Camerti*, 1, 29-35.

BINI, A., CITA, M.B. & GAETANI, M. (1978) Southern Alpine lakes – Hypotesys of an erosional origin related to the Messinian entrenchment. *Marine Geology*, 27, 271-188.

BLANC, P.L. (2000) Of sills and straits: a quantitative assessment of the Messinian Salinity Crisis. Deep-Sea Res., Part 1, *Oceanogr. Res. Pap*, 47-8, 1429–1460.

BLANC, P.L. (2006) Improved modelling of the Messinian Salinity Crisis and conceptual implication. *Palaeogeography, Palaeoclimatology, Palaeoecology*, 238, 349–372.

BLANC-VALLERON, M.M., PIERRE, C., CAULET, J.P., CARUSO, A., ROUCHY, J.M., CESPUGLIO, G., SPROVIERI, R., PESTREA, S. & DI STEFANO, E. (2002) Sedimentary, stable isotope and micropaleontological records of paleoceanographic change in the Messinian Tripoli Formation (Sicily, Italy). *Palaeogeography, Palaeoclimatology, Palaeoecology*, 185, 255–286.

BRESCIANI, I. & PEROTTI, C.R. (2014) An active deformation structure in the Po Plain (N Italy): The Romanengo anticline. *Tectonics*, 33, 2059-2076.

BUTLER, W.H.R., LICKORISH, W.H., GRASSO, M. & PEDLEY, H.M. (1995) Tectonics and sequence stratigraphy in Messinian basins, Sicily: Constraints on the initiation and termination of the Mediterranean salinity crisis. *GSA Bulletin*, 107, 425–439.

CAMESELLE, A. & URGELES R. (2016) Large-scale margin collapse during Messinian early sea-level drawdown: the SW Valencia trough, NW Mediterranean. *Basin Research,* 29, 576-595.

CARMINATI, E., LUSTRINO, M., CUFFARO, M., DOGLIONI, C. (2010) Tectonics, magmatism and geodynamics of Italy: what we know and what we imagine. In: Marco Beltrando, Angelo Peccerillo, Massimo Mattei, Sandro Conticelli and Carlo Doglioni, *Journal of the Virtual Explorer,* 36 (9).

CARUSO, A., PIERRE, C., BLANC-VALLERON, M.M. & ROUCHY, J.M. (2015) Carbonate deposition and diagenesis in evaporitic environments: The evaporative and sulphur-bearing limestones during the settlement of the Messinian Salinity Crisis in Sicily and Calabria. *Palaeogeography, Palaeoclimatology, Palaeoecology*, 429, 136-162.

CHUMAKOV, I.S., (1973) Pliocene and Pleistocene deposits of the Nile valley in Nubia and upper Egypt. In: *Initial Reports of the Deep Sea Drilling Project* (W.B.F. Ryan, K.J. Hsu¨ , et al., eds), 13, 1242–1243. *US Govern. Print. Office, Washington, DC.*

CIESM (Antón, J., Çağatay, M.N., De Lange, G., Flecker, R., Gaullier, V., Gunde-Cimerman, N., Hübscher, C., Krijgsman, W., Lambregts, P., Lofi, J., Lugli, S., Manzi, V., McGenity, T.J., Roveru, M., Sierro, F.J., & Suc, J.-P.) (2008) Executive Summary, in: Briand, F. (Ed.), *The Messinian Salinity crisis from mega-deposits to microbiology - A consensus report*. *CIESM Workshop Monographs*, Monaco, 7-28.

CITA, M.B. & CORSELLI, C. (1990) Messinian paleogeography and erosional surfaces in Italy: an overview. *Palaeogeography*, *Palaeoclimatology*, *Palaeoecology*, 77, 67-82.

CLAUZON, G. (1982) Le canyon messinien du Rhoˆne: Une preuve de´cisive du "dessicated deep basin model" (Hsu¨, Cita et Ryan, 1973) *Bull. Soc. Geol. Fr.,* 24, 231–246.

CLAUZON, G., SUC, J.P., GAUTIER, F., BERGER, A. & LOUTRE, M. (1996) Alternate interpretation of the Messinian salinity crisis: controversy resolved?. *Geology*, 24, 363–366.

CLAUZON, G., SUC, J.P, POPESCU, S.M, MARUNTEANU, M., RUBINO, J.L., MARINESCU, F. & MELINTE M.C (2005) Influence of Mediterranean sea-level changes on the Dacic Basin (Eastern Paratethys) during the late Neogene: the Medirettanan Lago Mare facies deciphered. *Basin Research,* 17, 437-462.

COSENTINO, D., BUCHWALDT, R., SAMPALMIERI, G., IADANZA, A., CIPOLLARI, P., SCHILDGEN, T. F., HINNOV, L. A., RAMEZANI, J. & BOWRING, S. A. (2013) Refining the Mediterranean "Messinian gap" with high-precision U-Pb zircon geochronology, central and northern Italy. *Geology*, 41, 323–326.

DE ALTERIIS, G. (1995) Different foreland basins in Italy: examples from the central and southern Adriatic Sea. *Tectonophysics*, 252, 349–373.

DE DONATIS, M. (2001) Three-dimensional visualization of the Neogene structures of an external sector of the Northern Apennine, Italy. *AAPG Bulletin*, 85-3, 419-431.

DEL BEN, A., GELETTI, R. & MOCNIK, A. (2010) Relationship between recent tectonics and inherited Mesozoic structures of the central-southern Adria plate. *Bollettino di Geofisica Teorica ed Applicata,* 51, 99-115.

DELA PIERRE, F., BERNARDI, E., CAVAGNA, S., CLARI, P., GENNARI, R., IRACE, A., LOZAR, F., LUGLI, S., MANZI, V., NATALICCIO, M., ROVERI, M. & VIOLANTI, D. (2011) The record of the Messinian salinity crisis in the Tertiary Piedmont basin (NW Italy): the Alba section revisited. *Paleogeography, Palaeoclimatology, Palaeoecology*, 30, 238-255.

DONDA, F., CIVILE, D., FORLIN, E., VOLPI, V., ZECCHIN, M., GORDINI, E., MERSON, B. & DE SANTIS, L. (2013) The northernmost Adriatic Sea: A potential location for CO_2 geological storage?. *Marine and Petroleum Geology*, 42, 148-159.

EBBING, J., BRAITENBERG, C. & GOTZE H. J. (2001). Forward and inverse modelling of gravity revealing insight into crust structures of the Eastern Alps. *Tectonophysics*, 337, 191-208.

FANTONI, R., MASSARI, F., MINERVINI, M., ROGLEDI, S. & ROSSI, M. (2001) Il messiniano del margine Sudalpino-Padano: relazioni tra contesto strutturale e stratigrafico-deposizionale. *Geol. Insubr.,* 6, 95–108

FANTONI, R., BERSEZIO R. & FORCELLA F. (2004) Alpine structure and deformation chronology at the Southern Alps-Po Plain border in Lombardy. *Boll. Soc. Geol. It*, 123, 463-476.

FANTONI, R. & FRANCIOSI, R. (2010) Mesozoic extension and Cenozoic compression in Po Plain and Adriatic foreland: Sassi, F.P. (Ed.), Nature and Geodynamics of the Lithosphere in Northern Adriatic. *Rend. Fis. Acc. Lincei*., 21, 181-196.

FINCKH, P.G. (1978) Are southern Alpine lakes former Messinian Canyons? Geophysical evidence for preglacial erosion in southern Alpine lakes. *Marine Geology*, 27, 289–302,

GARCIA-CASTELLANOS, D., Interplay between lithospheric flexure and river transport in foreland basins. *Basin Research,* 14 (2), 89-104.

GARCIA-CASTELLANOS, D., VERGÉS, J., GASPAR-ESCRIBANO, J., & CLOETINGH, S. (2003) Interplay between tectonics, climate, and fluvial transport during the Cenozoic evolution of the Ebro Basin (NE Iberia). *Journal of Geophysical Research*, 108, 2347.

GARGANI, J. (2004) Modelling of the erosion in the Rhone Valley during the Messinian crisis (France). *Quaternary International*, 121, 13–22.

GARGANI, J. & RIGOLLET, C. (2007) Mediterranean Sea-level variations during the Messinian salinity crisis. *Geophysical Research Letters*, 34, L10405.

GENNARI, R., MANZI, V., ANGELETTI, L., BERTINI, A., BIFFI, U., CEREGATO, A., FARANDA, C., GLIOZZI, E., LUGLI, S., MENICHETTI, E., ROSSO, A. & ROVERI, M. (2013) A shallow water record of the onset of the Messinian salinity crisis in the Adriatic foredeep (Legnagnone section, northern Apennines). *Palaeogeography, Palaeoclimatology, Palaeoecology*, 386, 145-164.

GHIELMI, M., MINERVINI, M., NINI, C., ROGLEDI, S. & ROSSI, M. (2010) Sedimentary and tectonic evolution in the eastern Po Plain and northern Adriatic Sea area from Messinian to Middle Pleistocene (Italy): Sassi, F.P. (Ed.), Nature and Geodynamics of the Lithosphere in Northern Adriatic. *Rend. Fis. Acc. Lincei*, 21, 131-166.

GHIELMI, M., MINERVINI, M., NINI C., ROGLEDI, S. & ROSSI M. (2013) Late Miocene-Middle Pleistocene sequences in the Po Plain - Northern Adriatic Sea (Italy): The stratigraphic record of modification phases affecting a complex foreland basin. *Marine and Petroleum Geology*, 42, 50-81.

GORINI, C., MONTADERT, L. & RABINEAU, M. (2015) New imaging of the salinity crisis: Dual Messinian lowstand megasequences recorded in the deep basin of both the eastern and western Mediterranean. *Marine and Petroleum Geology*, 66, 278-294.

GOVERS, R., MEIJER P. & KRIJGSMAN, W. (2009) Regional isostatic response to Messinian Salinity Crisis events. *Tectonophysics*, 463, 109-129.

HSÜ, K. J., CITA, M. B. & RYAN, W.B.F. (1973). Origin of the Mediterranean evaporites. *In: Ryan, W.B.F. and Hsü, K. J., Eds. Initial Reports of the Deep Sea Drilling Project,* 13, 1203-1231.

HSÜ, K.J., MONTADERT, L., BERNOULLI, D., CITA, M.B., ERICKSON, A., GARRISON, R.E., KIDD, R.B., MÈLIERÉS, F., MÜLLER, C. & WRIGHT, R. (1977) History of the Mediterranean Salinity Crisis. *Nature*, 267, 399-403.

ISPRA (2015) Modello geologico 3D e geopotenziali della Pianura Padana centrale (Progetto GeoMol). *Rapporti* ISPRA, 234/2015, pp. 104 e Appendice.

JOLIVET, L., AUGIER, R., ROBIN, C., SUC, JP. & ROUCHY, J.M. (2006) Lithospheric-scale geodynamic context of the Messinian salinity crisis. *Sedimentary Geology*, 188–189, 9–33.

KROON, I. (2002) Strength of the Adriatic lithosphere: inference from tectonic modelling [Ph.D. thesis]. *Amsterdam, The Netherlands, Vrije University*, p. 105.

KRIJGSMAN, W., HILGEN, F. J., RAFFI, I., SIERRO, F.J. & WILSON, D.S., (1999) Chronology, causes and progression of the Messinian salinity crisis. *Nature*, 400, 652–655.

KRIJGSMAN, W. & MEIJER, P.T. (2008) Depositional environments of the Mediterranean "Lower Evaporites" of the Messinian salinity crisis: constraints from quantitative analyses. *Marine Geology*, 253, 73–81.

KRUSE, S. & ROYDEN, L. (1994) Bending and unbending of an elastic lithosphere: the Cenozoic history of the Apennine and Dinaride foredeep basins. *Tectonics*, 13 (2), 278-302.

LIVIO, F.A., BERLUSCON, A., MICHETTI, A.M., SILEO, G., ZERBONI, A., TROMBINO, L., CREMASCHI, M., MUELLER, K., VITTORI, E., CARCANO, C. & ROGLEDI, S. (2009) Active fault-related folding in the epicentral area of the December 25, 1222 (Io=IX MCS) Brescia earthquake (Northern Italy): Seismotectonic implications. *Tectonophysics*, 476, 320–335.

LOFI, J., GORINI, C., BERNÉ, S., CLAUZON, G., DOS REIS, A. T., RYAN, W.B.F., MICHAEL, S., & STECKLER, M.S. (2005) Erosional processes and paleo-environmental changes in the Western Gulf of Lions (SW France) during the Messinian Salinity Crisis. *Marine Geology*, 217, 1-30.

LOFI, J., DÉVERCHÈRE, J., GAULLIER, V., GILLET, H., GUENNOC, P., GORINI, C., LONCKE, L., MAILLARD, A., SAGE, F. & THINON, I. (2011a) Seismic atlas of the Messinian salinity crisis markers in the offshore Mediterranean domain, CCGM. *Mémoires. Société Géologique de France,* 179, pp. 72.

LOFI, J., SAGE, F., DÉVERCHÈRE, J., LONCKE, L., MAILLARD, A., GAULLIER, V., THINON, I., GILLET, H., GUENNOC, P. & GORINI, C. (2011b) Refining our knowledge of the Messinian salinity crisis records in the offshore domain through multi-site seismic analysis. *Bull. Soc. géol. Fr.*, 182, 163-180.

LOGET, N., VAN DEN DRIESSCHE J. & DAVY P. (2005) How did the Messi- nian salinity crisis end? *Terra Nova*, 17, 414–419.

LOGET, N., DAVY, P. & VAN DEN DRIESSCHE J. (2006) Mesoscale fluvial erosion parameters deduced from modelling the Mediterranean sea-level drop during the Messinian (late Miocene). *Journal of Geophysical Research*, 111, F03005.

LYMER, G., LOFI, J., GAULLIER, V., MAILLARD, A., THINNON, I., SAGE, F., CHANIER, F. & VENDEVILLE, B.C. (2018) The Western Tyrrhenian Sea revised: New evidence for a rifted basin during the Messinian Salinity Crisis. *Marine Geology*, 398, 1-21.

MAESANO, F.E., D'AMBROGI, C., BURRATO, P. & TOSCANI, G. (2015) Slip-rates of blind thrust in slow deforming areas: examples from the Po Plain (Italy). *Tectonophysics*, 643, 8-25.

MAILLARD, A. & MAUFFRET, A. (2006) Relationship between erosion surfaces and Late Miocene Salinity Crisis deposits in the Valencia Basin (northwestern Mediterranean): evidence for an early sea-level fall. *Terra Nova,* 18, 321–329.

MANTOVANI, E., VITI, M., BABBUCCI, D., TAMBURELLI, C., CENNI, N., BAGLIONE, M. & D'INTINOSANTE, V. (2014) Generation of Back-Arc Basins as Side Effect of Shortening Processes: Example from the Central Mediterranean. *International Journal of Geosciences*, 5, 1062-1079.

MANZI, V., LUGLI, S., RICCI LUCCHI, F. & ROVERI, M. (2005) Deep-water clastic evaporites deposition in the Messinian Adriatic foredeep (northern Apennines, Italy): did the Mediterranean ever dry out?. *Sedimentology*, 52, 875-902.

MANZI, V., GENNARI, R., HILGEN, F., KRIJGSMAN, W., LUGLI, S., ROVERI, M. & SIERRO, F.J. (2013) Age refinement of the Messinian salinity crisis onset in the Mediterranean. *Terra Nova*, 25, 315-322.

MATANO, F., CRITELLI, S., BARONE, M., MUTO, F. & DI NOCERA, S. (2014) Stratigraphic and provenance evolution of the Southern Apennines foreland basin system during the Middle Miocene to Pliocene (Irpinia-Sannio successions, Italy). *Marine and Petroleum Geology,* 57, 652-670.

MEIJER, P.T., SLINGERLAND, R. & WORTEL M.J.R (2004) Tectonic control on past circulation of the Mediterranean Sea: a model study of the Late Miocene. *Paleoceanography*, 19, PA1026.

MEIJER, P.T. & KRIJGSMAN, W. (2005) A quantitative analysis of the desiccation and re-filling of the Mediterranean during the Messinian Salinity Crisis. *Earth and Planetary Science Letters*, 240, 510–520.

MICALLEF, A., CAMERLENGHI A., GARCIA-CASTELLANO, D., CUNARRO OTERO, D., GUTSCHER M.A., BARRECA, G., SPATOLA, D., FACCHIN, L., GALETTI, R., KRASTEL, S., GROSS, F. & URLAUB, M. (2018) Evidence of Zanclean megaflood in the eastern Mediterranean Basin. *Scientific Reports*, 8, 1078.

MILLER, K.G., KOMINZ, M.A., BROWING, J.V., WRIGHT, J.D., MOUNTAIN, G.S., KATZ, M.E., SUGARMAN, P.J., CRAMER, B.S., CHRISTIE-BLICK, N. & PEKAR, S.F. (2005) The Phanerozoic Record of Global Sea-Level Change. *Science, New Series*, 310, 1293-1298.

MOLINARI, I., ARGNANI, A., MORELLI, A. & BASINI, P. (2015) Development and testing of a 3D seismic velocity model of the Po Plain sedimentary basin, Italy. *Bulletin of the Seismological Society of America*, 105 (2), p. 753-764

MORETTI, I. & ROYDEN, L. (1988) Deflection, gravity anomalies and tectonics of doubly subducted continental lithosphere: Adriatic and Ionian Seas. *Tectonics*, 7, 875-893.

MOSCA, P. (2006) Neogene basin evolution in the Western Po Plain (NW Italy): Insights from seismic interpretations, subsidence analysis and low (U-Th)/He thermochronology: [Ph.D. thesis]. *Amsterdam, The Netherlands, Vrije University*, p. 167.

MÜLLER, D.W. & MUELLER, P.A (1991) Origin and age of the Mediterranean Messinian evaporates: implications from Sr isotopes. *Earth and Planetary Science Letters*, 107, 1-12.

PATACCA, E. & SCANDONE, P. (2007) Geology of the Southern Apennines. *Boll. Soc. Geol. It. (Italian Journal of Geoscience)*, 7, 75-119.

PELLEN, R., POPESCU SM., SUC JP. MELINTE-DOBRINESCU M. C., RUBINO JL., RABINEAU M., MARABINI S., LOGET N., CASERO P., CAVAZZA W., HEAD M. J., ASLANIAN D. (2017) The Apennine foredeep (Italy) during the latest Messinian: Lago Mare reflects competing brackish and marine conditions based on calcareous nannofossils and dinoflagellate cysts. *Geobios*, 50, 237-257.

PEROTTI, C. R. (1991) Osservazioni sull'assetto strutturale del versante padano dell'Appennino Nord-Occidentale. *Atti Ticinensi di Scienze della Terra*, 34, 11-22.

PIERI, M. & GROPPI, G. (1981) Subsurface geological structure of the Po Plain (Italy). *C.N.R.*

Progetto Finalizzato Geodinamica, 414, 1-13.

PIKELJ, K., HERNITZ-KUČENJAK, M., AŠČIĆ, Š. & JURAČIĆ, M. (2015) Surface sediment around the Jabuka Islet and the Jabuka Shoal: evidence of Miocene tectonics in the Central Adriatic Sea. *Marine Geology*, 359, 120-133.

RIZZINI, A. & DONDI, L. (1978) Erosional surface of Messinian age in the subsurface of the Lombardian Plain (Italy). *Marine Geology*, 27, 303-325.

ROYDEN, L. (1988) Flexural behaviour of the continental lithosphere in Italy: constraints imposed by gravity and deflection data. *Journal of Geophysical Research*, 93, B7, 7747-7766.

ROSSI, M. (2017) Outcrop and seismic expression of stratigraphic patterns driven by accommodation and sediment supply turnarounds: Implications on the meaning and variability of unconformities in syn-orogenic basins. *Marine and Petroleum Geology*, 87, 112-127.

ROSSI, M., ROGLEDI, S., BARBACINI, G., CASADEI, D., IACCARINO, S. & PAPANI, G. (2002) Tectono-stratigraphic architecture of Messinian piggyback basins of Northern Apennines: the Emilia folds in the Reggio-Modena area and comparison with Lombardia and Romagna sectors. *Boll. Geol. It.,* 1, 437-447.

ROSSI, M., MINERVINI, M., GHIELMI, M., & ROGLEDI, S. (2015) Messinian and Pliocene erosional surfaces in the Po Plain-Adriatic Basin: Insights from allostratigraphy and sequence stratigraphy in assessing play concepts related to accommodation and gateway turn arounds in tectonically active margins. *Marine and Petroleum Geology*, 66, 192-216.

ROSSI, M., MINERVINI, M. & GHIELMI, M. (2018) Drowing unconformities on hinged clastic shelves. *Geology,* doi.org/10.1130/G40123.1

ROUCHY, J.M. & CARUSO, A. (2006) The Messinian salinity crisis in the Mediterranean basin: a reassessment of the data and an integrated scenario. *Sedimentary Geology*, 188, 35-67.

ROVERI, M., MANZI, V., BERGAMASCO, A., FALCIERI, F.M., GENNARI, R., LUGLI, S. & SCHREIBER, C. (2014a) Dense shelf water cascading and Messinian canyons: a new scenario for the Mediterranean salinity crisis. *American Journal of Science*, 34, 751-784.

ROVERI, M., FLECKER, R., KRIJGSMAN, W., LOFI, J., LUGLI, S., MANZI, V., SIERRO, F.J., BERTINI, A., CAMERLENGHI, A., DE LANGE, G., GOVERS, R., HILGEN, F.J., HÜBSCHER, C., MEIJER, P.T.H. & STOICA, M. (2014b) The Messinian Salinity Crisis: Past And Future Of A Great Challenge For Marine Sciences. *Marine Geology*, 352, 25–58.

ROVERI, M., GENNARI, R., LUGLI, S., MANZI, V., MINELLI, N., REGHIZZI, M., RIVA, A., ROSSI, M. & SCHREIBER B.C. (2016) The Messinian salinity crisis: open problems and possible implications for Mediterranean petroleum systems. *Petroleum Geoscience*, 22, 283-290.

RYAN, W.B.F., (1976) Quantitative evaluation of the depth of the western Mediterranean before, during and after the Late Miocene salinity crisis. *Sedimentology*, 23, 791-813.

RYAN, W.B.F., (2009) Deconding the Mediterranean salinity crisis. *Sedimentology,* 56, 95-136.

RYAN, W.B.F. & CITA, M.B. (1978) The nature and distribution of Messinian Erosional Surfaces; indicators of a several-kilo- meter-deep Mediterranean in the Miocene. *Marine Geology*, 27, 193–230.0

SANTANTONIO, M., SCROCCA, D. AND LIPPARINI, L. (2013) The Ombrina-Rospo Plateau (Apulian Platform): Evolution of a Carbonate Platform and its Margins during the Jurassic and Cretaceous. *Marine Petroleum Geology*, 42, 4-29.

SCHILDGEN, T. F., COSENTINO, D., FRIJIA, G., CASTORINA, F., DUDAS, F.Ö., IADANZA, A., SAMPALMIERI, G., CIPOLLARI, P., CARUSO, A., BOWRING, S.A. & STRECKER, M.R. (2014) Sea-level and climate forcing of the Sr isotope composition of late Miocene Mediterranean marine basins. *Geochem. Geophys. Geosyst.*, 15, 2964–2983.

SCISCIANI, V. & CALAMITA, F. (2009) Active intraplate deformation within Adria: Examples from the Adriatic region. *Tectonophysics*, 476, 57-72.

SCLATER, J.B & CRISTIE P.A.F (1980) Continental stretching: an explanation of the post-mid-cretaceous subsidence of the central North Sea basin. *Journal of Geophysical Research,* 85, 3711-3739.

SCROCCA, D. (2010) Southern Apennines: structural setting and tectonic evolution: (Eds.) Marco Beltrando, Angelo Peccerillo, Massimo Mattei, Sandro Conticelli, and Carlo Doglioni. *Journal of the Virtual Explorer*, 36, 13.

SCROCCA, D., CARMINATI, E., DOGLIONI, C. & MARCANTONI, D. (2007) Slab Retreat and Active Shortening along the Central-Northern Apennines. In: Lacombe O., Roure F., Lavé J. and Vergés J. (eds.), *Thrust Belts and Foreland Basins: SE-25, Frontiers in Earth Sciences. Springer Berlin Heidelberg*, 471-487.

SELLI, R. (1960) Il Messiniano Mayer-Eymar, 1867, Proposta di un neostratotipo. *Giornale di Geologia*, 28, 1-33.

SIERRO, F.J., HILGEN, F.J., KRIJGSMAN, W. & FLORES, J.A. (2001) The Abas composite (SE Spain): a Messinian reference section for the Mediterranean and the APTS. *Palaeogeography*, *Palaeoclimatology*, *Palaeoecology*, 168, 141-169.

STAMPFLI, G.M. & HOCKER, C.F. (1989) Messinian paleorelief from a 3-D seismic survey in the Tarraco concession area (Spanish Mesiterranean-Sea). *Geol. en Mijnb.,* 68, 201–210.

STERNAI, P., HERMAN F., CHAMPAGNAC, J.D, FOX, M., SALCHER, B. & WILLETT, S.D. (2012) Pre-glacial topography of the European Alps. *Geology*, 40, 1067-1070.

STERNAI, P., CARICCHI, L., JOLIVET, L., GARCIA-CASTELLANOS, D., SHELDRAKE, T. & CASTELLTORT, S. (2017) Magmatic pulse driven by sea-level changes associated with the Messinian Salinity Crisis. *Nature Geoscience*, 10, 783-787.

THINON, I., GUENNOC, P., SERRANO, O., MAILLARD, A., LASSEUR, E. & RÉHAULT, J.P. (2016) Seismic markers of the Messinian Salinity Crisis in an intermediate-depth basin: data for understanding the Neogene evolution of the Corsica Basin (Northern Tyrrhenian Sea). *Marine and Petroleum Geology.* 77, 1274-1296.

TOSCANI, G., BONINI, L., AHMAD, M.I., BUCCI, D.D., DI GIULIO, A., SENO, S. & GALUPPO, C. (2014) Opposite verging chains sharing the same foreland: Kinematics and interactions through analogue models (Central Po Plain, Italy). *Tectonophysics*, 633, 268-282.

TOSCANI, G., MARCHESINI, A., BARBIERI, C., DI GIULIO, A., FANTONI, R., MANCIN, N. & ZANFERRARI, A. (2016) The Friulian-Venetian Basin I: architecture and sediment flux into a shared foreland basin. *Ital. J. Geosci.*, 135, 444-459.

TURRINI, C., LACOMBE, O. & ROURE, F. (2014) Present-day 3D structural model of the Po Valley basin, Northern Italy. *Marine and Petroleum Geology*, 56, 266-289.

TURRINI, C., TOSCANI, G., LACOMBE, O. & ROURE, F. (2016) Influence of structural inheritance on foreland-foredeep system evolution: An example from the Po valley region (northern Italy). *Marine and Petroleum Geology*, 77, 376-398.

URGELES, R., CAMERLENGHI, A., GARCIA-CASTELLANOS, D., DE MOL, B., GARCÉS, M., VERGÉS, J., HASLAM I. & HARDMAN, M. (2011) New constraints on the Messinian sealevel drawdown from 3D seismic data of the Ebro Margin, western Mediterranean. *Basin Research*, 23, 123-145.

VAI, G.B. (2016) Over half a century of Messinian salinity crisis. *Boletin Geologico y Minero*, 127, 625-641.

VELIĆ, J., MALVIĆ, T., CVETKOVIĆ, M. & VELIĆ, I. (2015) Stratigraphy and petroleum geology of the Croatian part of the Adriatic basin. *J. Pet. Geol.*, 38, 281–300.

ZECCHIN, M., DONDA, F. & FORLIN, E. (2017) Genesis of the Northern Adriatic Sea (Northern Italy) since early Pliocene. *Mar. Petr. Geol.*, 79, 108-130.

Web Site

ViDEPI Project, http://www.videpi.com

GTOPO30, https://lta.cr.usgs.gov/GTOPO30

FIGURE CAPTIONS

FIGURE 1

A: Tectonic map of the study area.

B: Geological section (a-a') along profile, modified from Toscani *et al*. (2014). See Fig. 1a for location.

C: Seismic profile in TWT (b-b') (see Fig. 1a for location) from Eni dataset from the Northern Apennines thrust-fold belt to the Southern Alps. Seismic data has European normal standard. Grayscale Amplitude in the range of ±18.00.

FIGURE 2

Cross correlation panel by well log analysis. PS (Spontaneous Potential), RES (Resistivity).

A: Red stars are wells from ViDEPI project showing the extended erosion and the complete lack of Messinian deposits. From NW to SE: Ornella 1, Glenda 1 and Alessandra 1 wells. See Fig. 1a for location.

B: White stars are wells from Eni private database showing late Messinian depocenter filled with post-evaporitic turbidites of the Fusignano Fm. overlying a syn-evaporitic sequence (gypsum and/or anhydrite) thinning towards the NE Adriatic foreland ramp. Note that electric logs data for the second well to the SW does not reach the bottom of the Plio-Pleistocene but the stratigraphic column includes 33 m of Messinian brackish fine deposits and 17 m of evaporites. See Fig. 1a for location.

FIGURE 3

A: Study area and complete dataset. Red lines correspond to the ENI seismic grid, while yellow lines correspond to the seismic profiles by public ViDEPI dataset. Black squares are drillings from both private and public database.

B: Area where the dataset has been integrated with observations from Fantoni *et al*. (2004), Mosca (2006), Bigi *et al*. (1992), Rossi (2017).

C: Area where the dataset has been integrated with observations from Toscani *et al*. (2016).

D: Area where the dataset has been integrated with observations from Fantoni *et al*. (2001).

FIGURE 4

A: Work flow used to restore the Messinian landscape during the maximum sea-level draw down.

B: Conceptual model of the backstripping procedure applied to the basin.

FIGURE 5

A: Current position of the main late-Messinian Northern Apennines and Southern Alps thrusts buried in the Po Plain (solid black lines) and Plio-Pleistocene thrust fronts (dashed black lines). Symbols and code name refer to the location of the main Plio-Pleistocene structures vertically restored (see Tab. 2).

B: Black lines show the current position of main late-Messinian Northern Apennines and Southern Alps thrusts buried in the Po Plain subsurface, compared with their restored late-Messinian position (red lines), according with shortening rates from the bibliography (see text for detail).

FIGURE 6

Map of the reconstructed MES with 500 m contouring with respect to the modern topography.

FIGURE 7

A: Map of the reconstructed MES in the central Southern Alps, zoom from figure 6, with 500 m contouring with respect to the modern topography. Blue lines show the present-day fluvial network.

B: Profile (in depth domain) along the trace a-a'. The black line is the present-day topography (vertically exaggerated) and the red line is the MES. Note the match between the locations of valleys on the modern topography and the MES.

C: Seismic profile along b-b' trace is from Eni private dataset. It shows some details of two canyons in the bedrock below the Po Plain. Note the good fit between the present-day Serio river location and the Messinian incision (MES) directly below. The green line (TES, as Top Erosion Surface) is a successive erosional phase (base Zanclean) that removed the most of the post-evaporitic fluvial gravels delta system (with high amplitude reflector facies). Only some remnants were preserved at the bottom valley and on top of interfluve. The paleo-valley is then sealed by Plio-Pleistocene turbidites. Blue line corresponds to the Intra-Zanclean Unconformity (I-ZU). Pre-Messinian deposits refer to the Oligo-Miocene succession.

FIGURE 8

Paleogeography obtained by modelling two extreme scenarios involving the same *Te* (20 km) and lithologic properties but (**A**) 200 m and (**B**) 1500 m MSC sea-level drawdown. Red contour lines are the corresponding calculated flexural uplift.

C, D, E: Shoreline migration produced by imposing different magnitude of sea-level drop and *Te* values. For these models, fixed lithologic properties were considered.

FIGURE 9

A: Restored late Messinian landscape, with 200 m contouring applying, from our preferred model accounting for a 850 m sea-level drop. The dotted black line shows the continental *vs* marine shelf-to-basin facies boundary by *Ghielmi et al.* (2010, 2013).

B: TWT amplitude colour map of the MES showing a subaerial drainage network (after Ghielmi *et al.*, 2010).

C: Seismic map (TWT) of the Messinian unconformity showing the dip morphological seismic attribute (after Ghielmi *et al.*, 2010, 2013 and Rossi, 2017). The pre-evaporitic shoreline break is highlighted in the northeast. Some NE-SW Pliocene incisions with retrogressive slump scars can be observed.

FIGURE 10

Map of the estimated isostatic uplift for our preferred model (*Te* 20 km and MSC sea-level drop of 850 m). White lines show the restored position of the main Northern Apennine and Southern Alpine thrust fronts during the late-Messinian.

TABLE 1 - Parameters for different lithologies from BasinMod2014 software and used for decompaction and uplift calculation.

TABLE 2 - Structure code-name and location in figure 5 from Maesano *et al*. (2015); geometric features of the fault and the vertical component considering the age interval of the tectonic activity (see Fig. 5a for location).

TABLE 3 - Table of maximum uplift variations under different input parameters: sediments porosity, *Te* and sea-level drops.

References	**Litholog y type**	**Lithology Mixing (%)**	**Porosity**	**Exp Compac.Coeff (1/km)**	**Grain Density (kg/m^3)**	**Bulk density (kg/m^3)**
Sclater & Christie, 1980	Sandston e	100% Sand	0,49	0,27	2650	2096
Sclater & Christie, 1980	Shale	100% Shale	0,63	0,51	2720	2140
Sclater & Christie, 1980	Shaley Sandston e	50% Sand 50% Shale	0,56	0,39	2680	2115
BasinMod 2014 library	Sandy Shales	75% Shale 25% Sand	0,563	0,45	2700	2149

Structure	**References**	**Fault dip**	**Total slip (m)**	**Age Interval (Ma)**	**Vertical component to be removed (m)**
MI	Scrocca et al., 2007	-	-	1.4 – 0	570
T5FF	Maesano et al., 2015	40°	1659	3.6 – 0	1059
T6FF	Maesano et al., 2015	25°	750	1.81 – 0	315
T9RF in	Maesano et al., 2015	30°	3178	3.6 – 0	1589
T9RF out	Maesano et al., 2015	30°	1425	3.6 – 0	815
T2EF	Maesano et al., 2015	40°	703	3.6 – 0	1400
T3EF	Maesano et al., 2015	40°	340	1.81 - 0	950
Romanengo Anticline (RA)	Bresciani & Perotti, 2014 Maesano et al., 2015	-	-	5.33 - 0	1150

Post-MES vol. Porosity	Pre-MES vol. Porosity	Te (km)	Uplift max (m) (-200 m drop)	Uplift max (m) (-850 m drop)	Uplift max (m) (-1500 m drop)
50sh-50s	75sh-25s	10	1109.6	1306.6	1452.1
50sh-50s	100%shale	10	1109.5	1303.3	1441
50sh-50s	100%sand	10	1109.7	1310.2	1467.3
50sh-50s	75sh-25s	20	829.7	994.9	1091.3
50sh-50s	100%shale	20	829.4	989.1	1079.7
50sh-50s	100%sand	20	830.1	1002.1	1108.5
50sh-50s	75sh-25s	45	488.7	603.4	654.4
50sh-50s	100%shale	45	488.3	599.7	646.9
50sh-50s	100%sand	45	489.2	608.3	665.7

Post-MES vol. Porosity	Pre-MES vol. Porosity	Te (km)	Uplift max (m) (-200 m drop)	Uplift max (m) (-850 m drop)	Uplift max (m) (-1500 m drop)
100%shale	75sh-25s	10	1133.7	1329.9	1473.4
100%shale	100%shale	10	1133.6	1326.4	1462
100%shale	100%sand	10	1133.8	1333.8	1488.9
100%shale	75sh-25s	20	847.4	1011.4	1106.6
100%shale	100%shale	20	847.1	1005.5	1094.8
100%shale	100%sand	20	847.8	1018.9	1124
100%shale	75sh-25s	45	498.9	604.5	663.6
100%shale	100%shale	45	498.5	600.9	656
100%shale	100%sand	45	499.4	609.4	674.9

Post-MES vol. Porosity	Pre-MES vol. Porosity	Te (km)	Uplift max (m) (-200 m drop)	Uplift max (m) (-850 m drop)	Uplift max (m) (-1500 m drop)
100%sand	75sh-25s	10	1091.3	1288.8	1435.9
100%sand	100%shale	10	1091.2	1285.7	1425
100%sand	100%sand	10	1091.4	1292.3	1450.8
100%sand	75sh-25s	20	816.3	982.3	1079.7
100%sand	100%shale	20	816	976.6	1068.1
100%sand	100%sand	20	816.7	989.2	1096.8
100%sand	75sh-25s	45	480.9	587.4	647.5
100%sand	100%shale	45	480.5	583.8	639.9
100%sand	100%sand	45	481.4	592.2	658.7

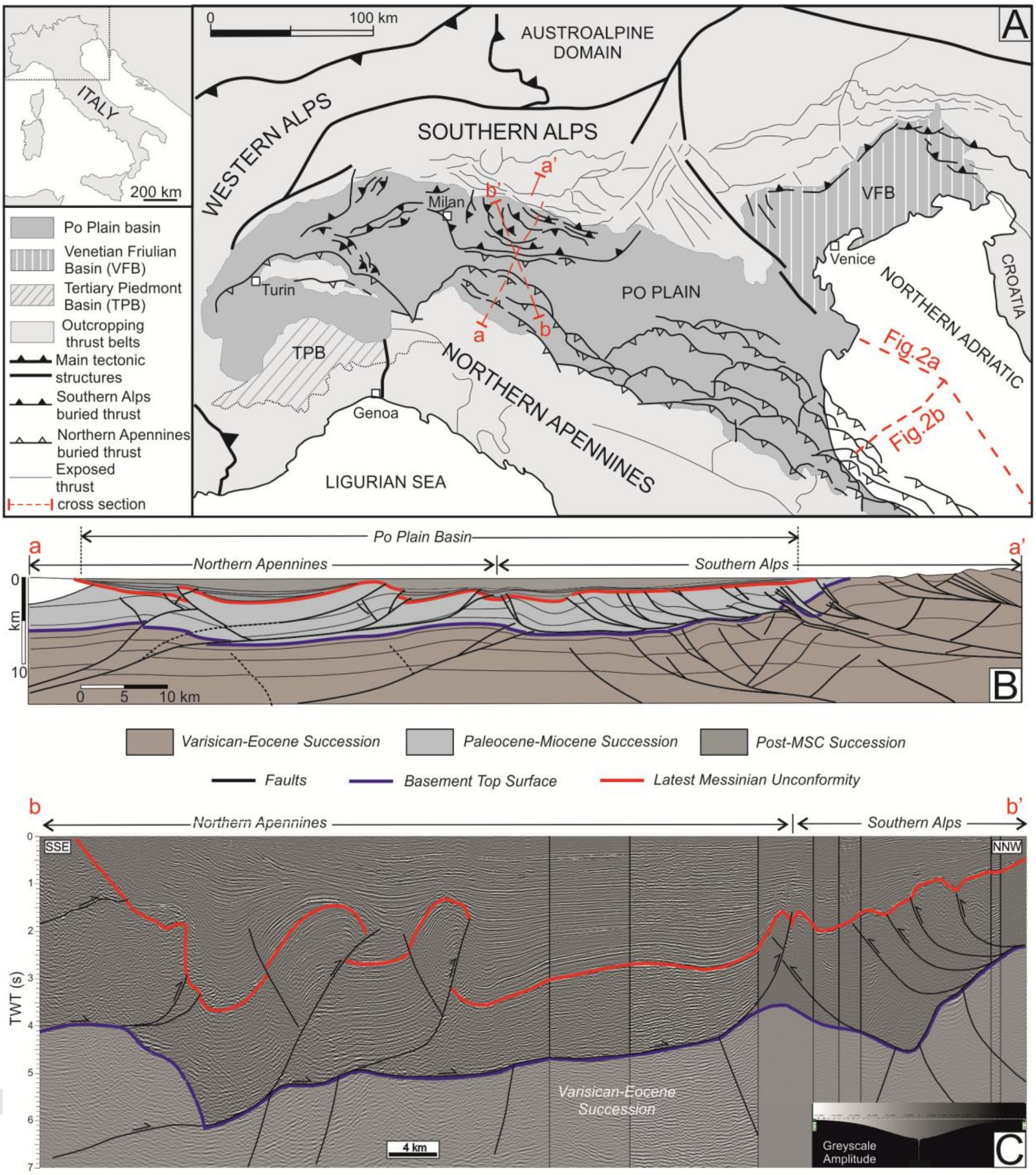
A
0
100 km
ITALY
200 km
AUSTROALPINE
DOMAIN
WESTERN ALPS
SOUTHERN ALPS
Milan
Turin
TPB
Genoa
LIGURIAN SEA
NORTHERN APENNINES
PO PLAIN
VFB
Venice
NORTHERN ADRIATIC
CROATIA
Fig.2a
Fig.2b
a
a'
b
b'
Po Plain basin
Venetian Friulian Basin (VFB)
Tertiary Piedmont Basin (TPB)
Outcropping thrust belts
Main tectonic structures
Southern Alps buried thrust
Northern Apennines buried thrust
Exposed thrust
cross section
B
Po Plain Basin
Northern Apennines
Southern Alps
km
0
10
0 5 10 km
Varisican-Eocene Succession
Paleocene-Miocene Succession
Post-MSC Succession
Faults
Basement Top Surface
Latest Messinian Unconformity
C
SSE
NNW
TWT (s)
Varisican-Eocene Succession
4 km
Greyscale Amplitude

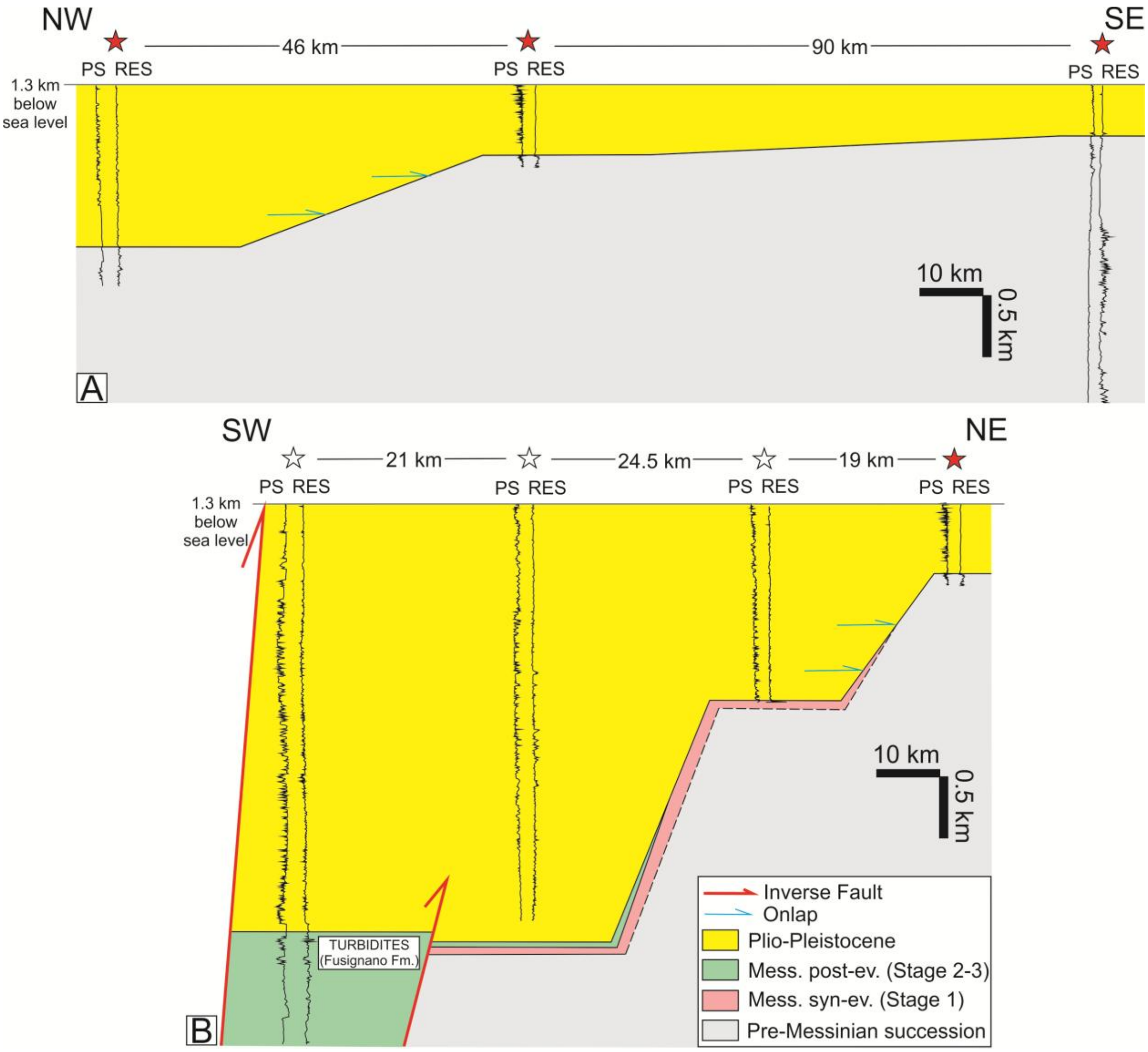

NW
46 km
90 km
SE
PS RES
PS RES
PS RES
1.3 km below sea level
10 km
0.5 km
A
SW
21 km
24.5 km
19 km
NE
PS RES
PS RES
PS RES
PS RES
1.3 km below sea level
TURBIDITES (Fusignano Fm.)
10 km
0.5 km
Inverse Fault
Onlap
Plio-Pleistocene
Mess. post-ev. (Stage 2-3)
Mess. syn-ev. (Stage 1)
Pre-Messinian succession
B

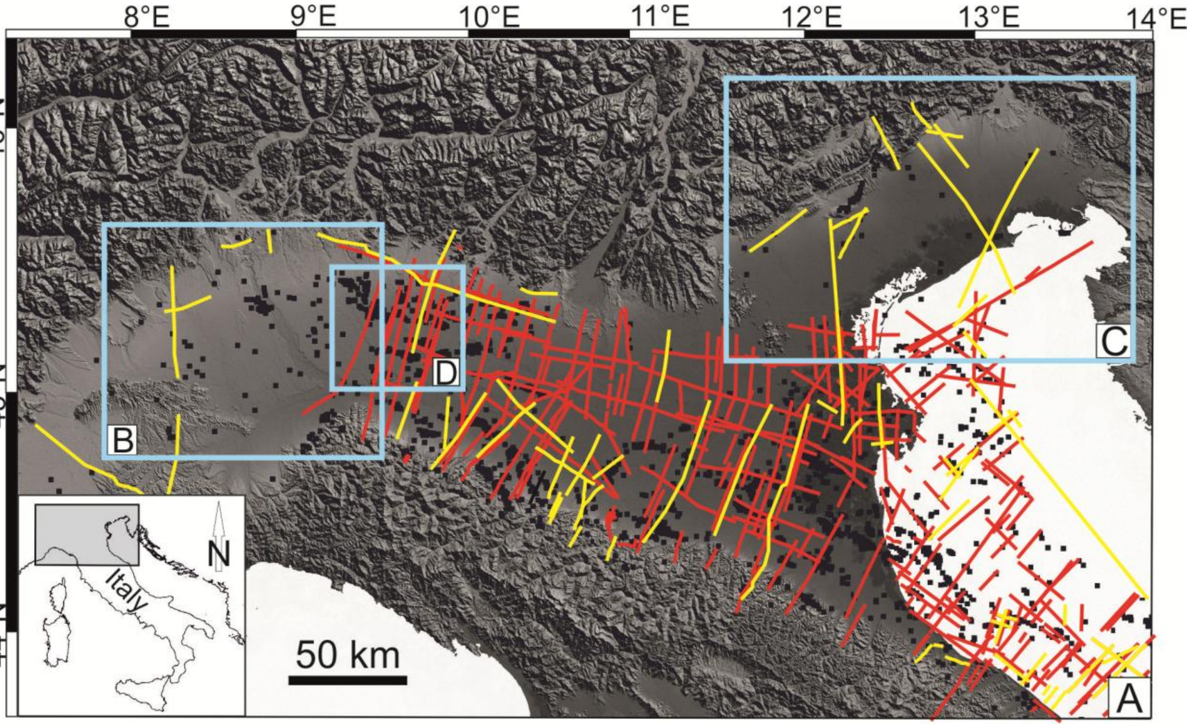
8°E
9°E
10°E
11°E
12°E
13°E
14°E
46°N
45°N
44°N
B
C
D
A
N
Italy
50 km

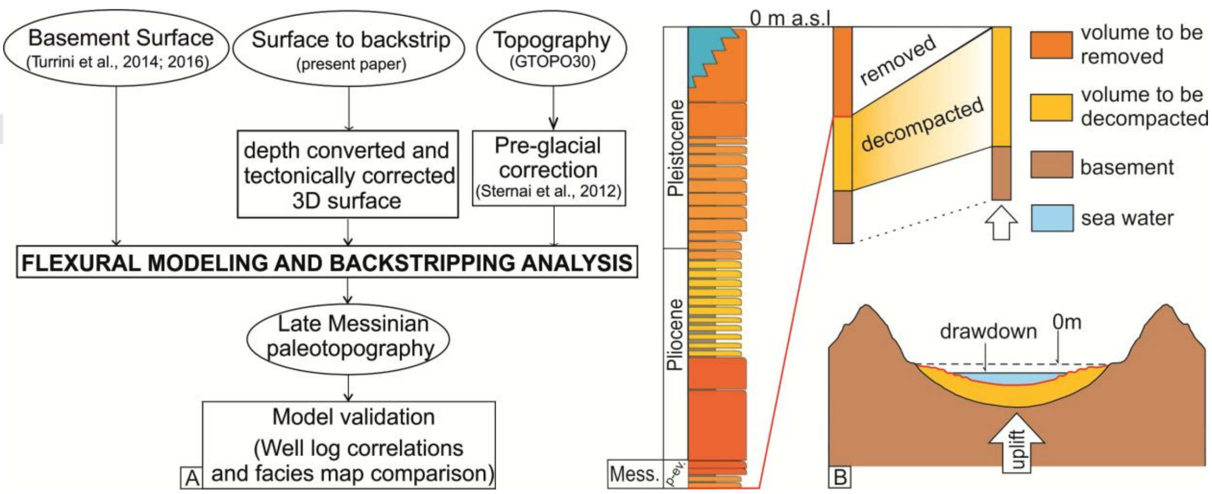
Basement Surface
(Turrini et al., 2014; 2016)
Surface to backstrip
(present paper)
Topography
(GTOPO30)
depth converted and tectonically corrected 3D surface
Pre-glacial correction
(Sternai et al., 2012)
FLEXURAL MODELING AND BACKSTRIPPING ANALYSIS
Late Messinian paleotopography
Model validation
(Well log correlations and facies map comparison)
A
0 m a.s.l
Pleistocene
Pliocene
Mess.
p-ev.
removed
decompacted
volume to be removed
volume to be decompacted
basement
sea water
drawdown
0m
uplift
B

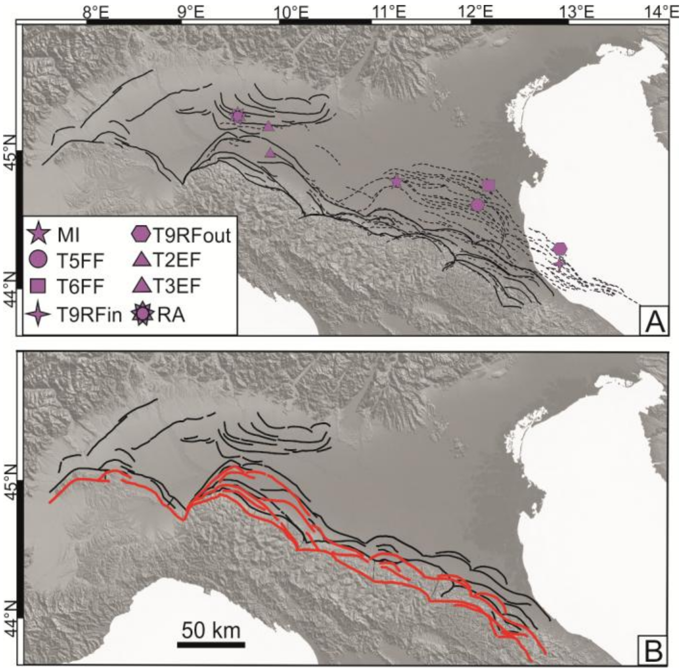
8°E
9°E
10°E
11°E
12°E
13°E
14°E
45°N
44°N
MI
T5FF
T6FF
T9RFin
T9RFout
T2EF
T3EF
RA
A
50 km
B

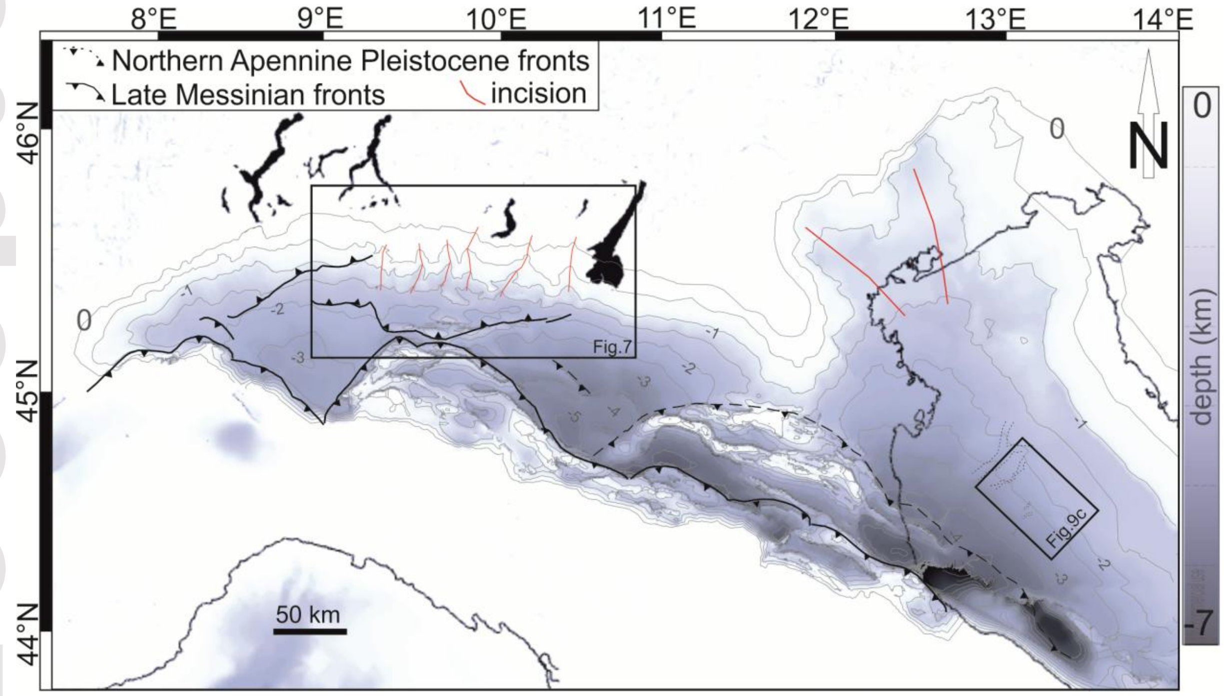
8°E
9°E
10°E
11°E
12°E
13°E
14°E
46°N
45°N
44°N
Northern Apennine Pleistocene fronts
Late Messinian fronts
incision
N
0
depth (km)
-7
Fig.7
Fig.9c
50 km

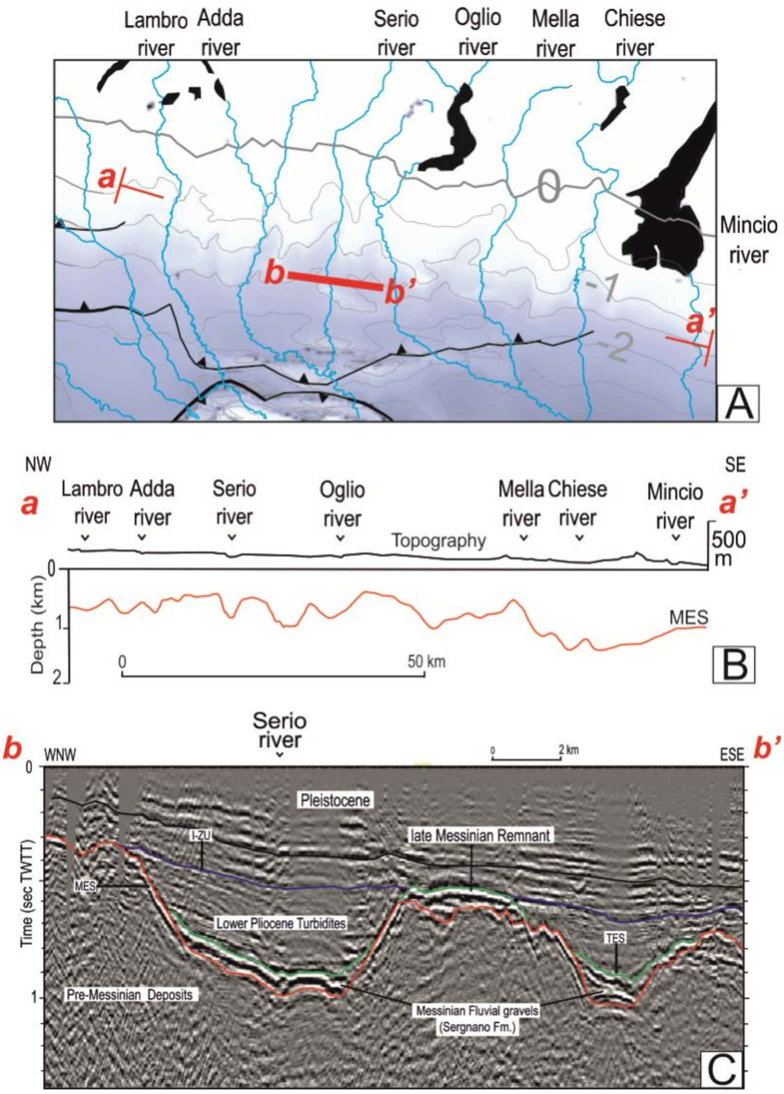
Lambro river
Adda river
Serio river
Oglio river
Mella river
Chiese river
Mincio river
a
a'
b
b'
0
-1
-2
A
NW
SE
Lambro river
Adda river
Serio river
Oglio river
Mella river
Chiese river
Mincio river
Topography
500 m
Depth (km)
MES
0
50 km
B
b
WNW
Serio river
ESE
b'
2 km
Pleistocene
I-ZU
late Messinian Remnant
MES
Lower Pliocene Turbidites
TES
Pre-Messinian Deposits
Messinian Fluvial gravels (Sergnano Fm.)
Time (sec TWTT)
C

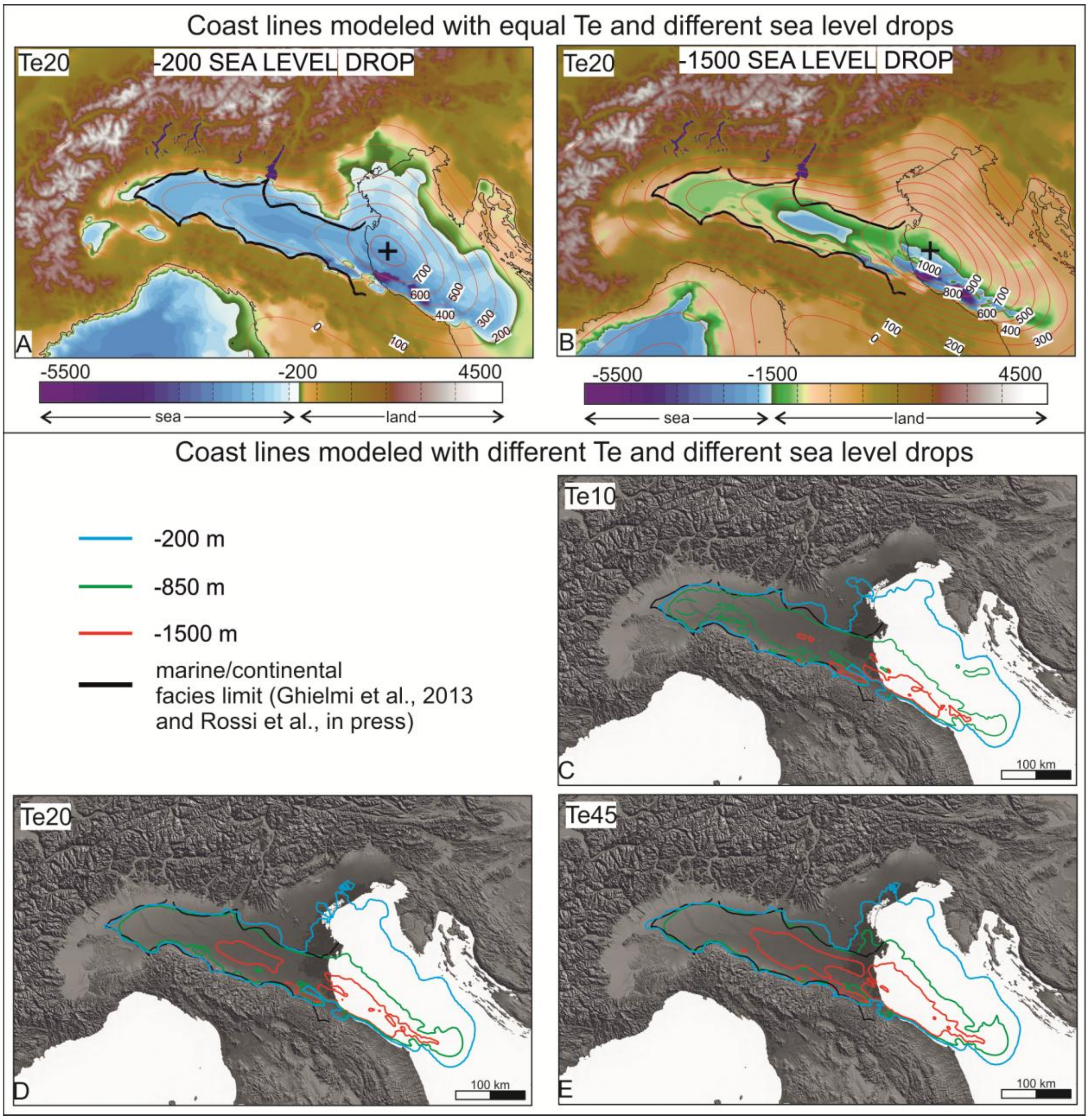
Coast lines modeled with equal Te and different sea level drops
Te20
-200 SEA LEVEL DROP
Te20
-1500 SEA LEVEL DROP
A
B
-5500
-200
4500
sea
land
-5500
-1500
4500
sea
land
Coast lines modeled with different Te and different sea level drops
-200 m
-850 m
-1500 m
marine/continental facies limit (Ghielmi et al., 2013 and Rossi et al., in press)
Te10
C
Te20
D
Te45
E
100 km

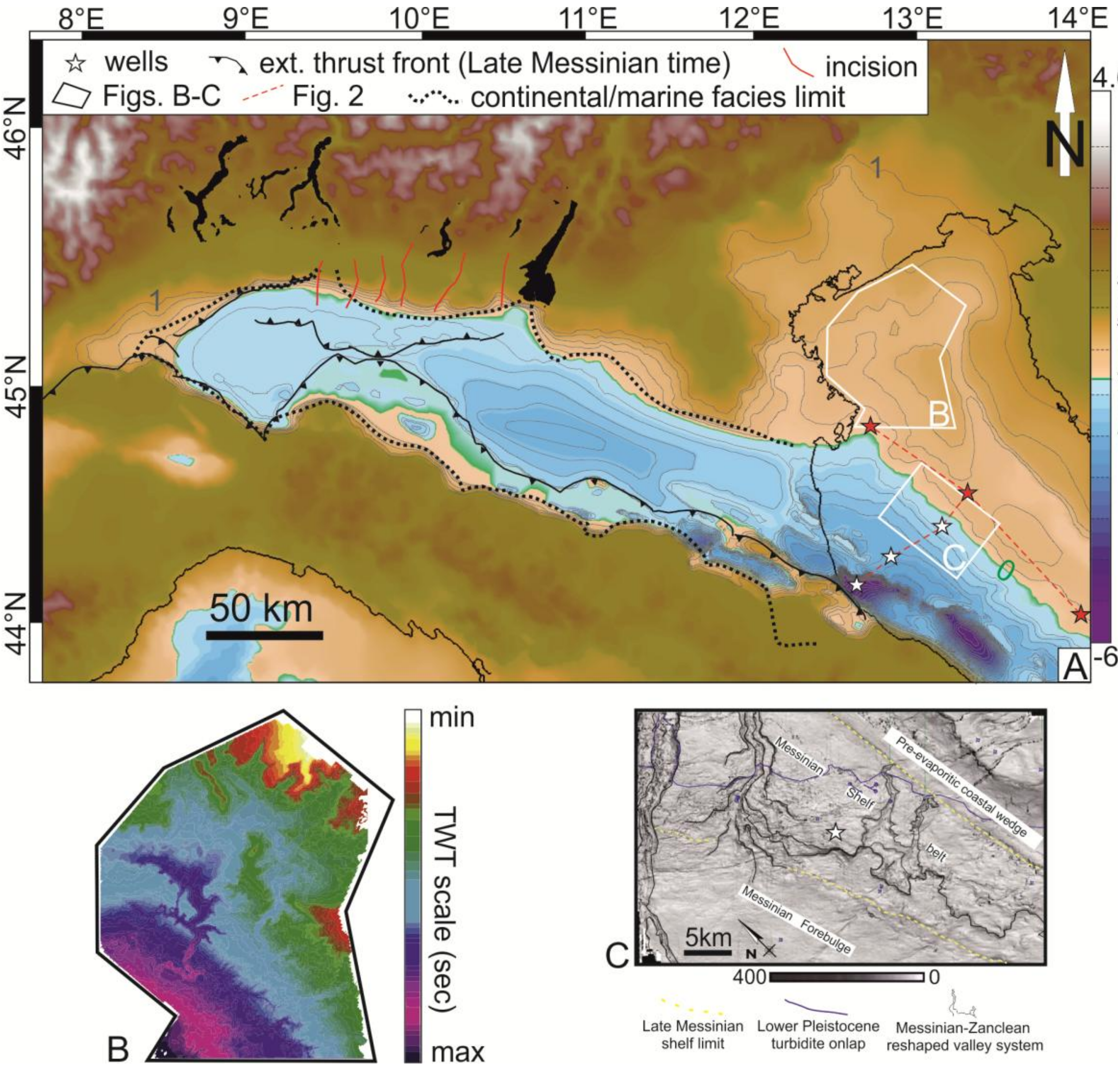
8°E
9°E
10°E
11°E
12°E
13°E
14°E
46°N
45°N
44°N
wells
ext. thrust front (Late Messinian time)
incision
Figs. B-C
Fig. 2
continental/marine facies limit
N
4.6
elevation (km)
-6
50 km
A
B
C
min
TWT scale (sec)
max
Messinian Shelf belt
Pre-evaporitic coastal wedge
Messinian Forebulge
5km
400
0
Late Messinian shelf limit
Lower Pleistocene turbidite onlap
Messinian-Zanclean reshaped valley system

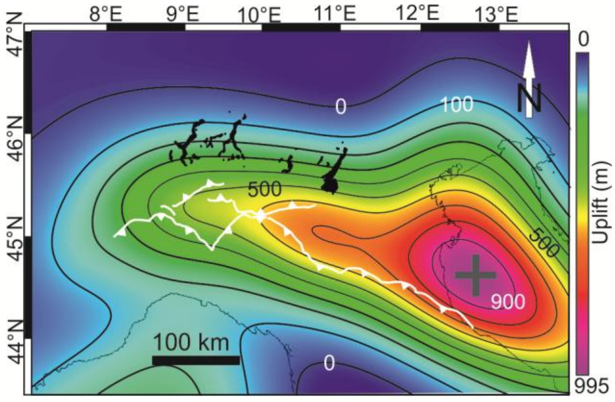
8°E
9°E
10°E
11°E
12°E
13°E
47°N
46°N
45°N
44°N
0
100
N
500
500
900
0
100 km
0
Uplift (m)
995